

PAPER



Cite this: DOI: 10.1039/d2dt01691e

Received 30th May 2022,
Accepted 18th June 2022

DOI: 10.1039/d2dt01691e

rsc.li/dalton

Coordination chemistry of hepta-*tert*-butylnonaphosphane†Volker Jens Eilrich,^a Toni Grell,^b Peter Lönnecke^a and Evamarie Hey-Hawkins^{*a}

Hepta-*tert*-butylnonaphosphane {*cyclo*-(P₄^tBu₃)₂}P^tBu was employed as a ligand in transition metal complexes of iron(0) (**1**), cobalt(–I) (**2**), copper(I) (**3**) and rhodium(I) (**4**), which are readily formed in moderate to good yields, and an unstable palladium(II) complex (**5**). The ligand features three different bonding modes (one monodentate (compounds **1** and **2**) and two bidentate (compounds **3–5**) with formation of four- or six-membered chelate rings), as determined by X-ray diffraction studies. The ³¹P{¹H} NMR spectral data of **1–3** have been determined by automated line-shape analysis.

Introduction

In analogy to carbon, phosphorus tends to build homonuclear scaffolds which display a wide variety of structural patterns. This phenomenon and other similarities—for instance the existence of isomers or valence tautomerism—can be rationalised by the concept of isolobality.^{1–3} One class of cyclic P_{*n*} frameworks is constituted by the cyclooligophosphanes *cyclo*-(P_{*n*}R_{*m*}) (*n* ≥ *m*) which are isolobal to cycloalkanes. Although a relatively large number of cyclooligophosphanes has been described^{2–5} and several metal carbonyl complexes are known,^{6–26} there are only a few examples of coordination compounds with other co-ligands than carbonyl.^{27–31} This fact is astonishing as compounds containing several phosphorus atoms with free lone pairs of electrons should be considered as ideal ligands in metal complexes due to the variety in coordination possibilities and the soft properties of phosphorus(III) according to the HSAB concept.³² Studies concerning {*cyclo*-(P₄^tBu₃)₂}³³ and its pentalane analogue³⁰ revealed their multifaceted coordination chemistry, displaying mono- to trimetallic complexes with six different coordination modes.^{29,30,34} Predominantly, monometallic chelate complexes of {*cyclo*-(P₄^tBu₃)₂} are observed with a wide range of metals. The octaphosphane ligand is, however, quite rigid, and this rigidity seemed to be a limiting factor for the scope of metal complexes to be formed. A more flexible cyclooligophosphane can be expected to display a more versatile coordination behaviour. Therefore, we have focussed on the

coordination chemistry of nonaphosphane {*cyclo*-(P₄^tBu₃)₂}P^tBu, which was first described by Baudler *et al.*, albeit with a reported yield of only 0.4%.³⁵

Results and discussion

We have previously reported an easy and straightforward preparation of {*cyclo*-(P₄^tBu₃)₂}P^tBu in our studies on activation of white phosphorus (P₄) with Li^tBu and the use of Li{*cyclo*-(P₄^tBu₃)} as a *cyclo*-(P₄^tBu₃) synthon.³⁶ Nonaphosphane {*cyclo*-(P₄^tBu₃)₂}P^tBu³⁶ (**L**) readily forms complexes with iron(0) ([Fe(CO)₄L] (**1**), cobalt(–I) ([Co(CO)₂(NO)L] (**2**)), copper(I) ([CuBr]₂L] (**3**)), rhodium(I) ([RhCl(CO)L] (**4**)), and palladium(II) ([PdCl₂L] (**5**)) (Scheme 1). Compounds **1–4** were fully characterised by spectroscopic methods and single-crystal X-ray diffraction, while complex **5** was only structurally characterised in the solid state by XRD. Complex formation with the corresponding octaphosphane was already reported for cobalt(–I), copper(I), rhodium(I) and palladium(II),²⁹ but not for iron(0) tetracarbonyl.

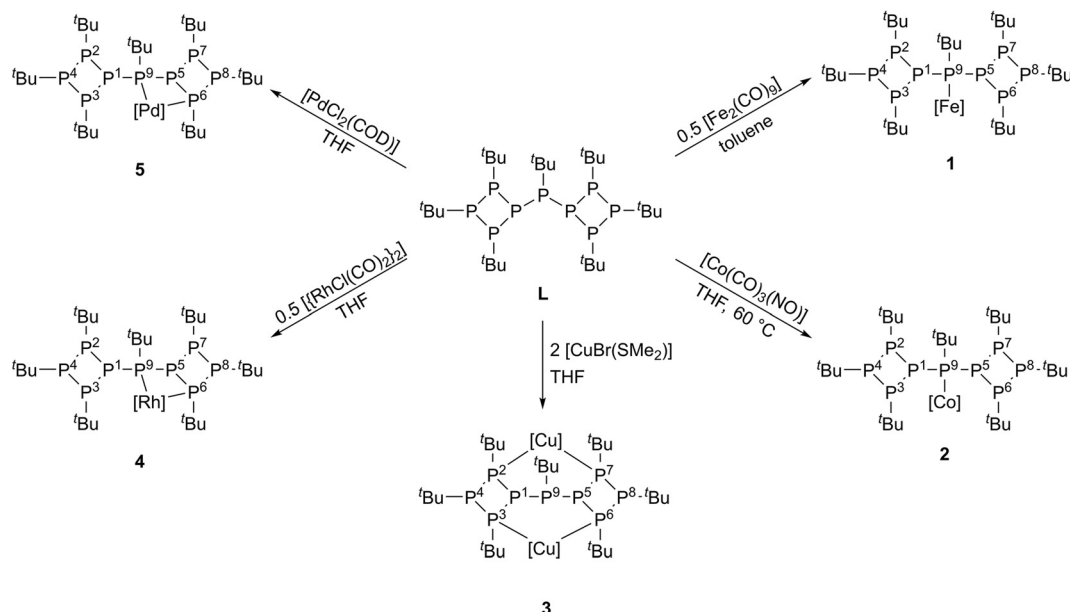
[Fe(CO)₄{*cyclo*-(P₄^tBu₃)₂}P^tBu-κP⁹] (**1**)

When nonaphosphane {*cyclo*-(P₄^tBu₃)₂}P^tBu (**L**) is added to a suspension of [Fe₂(CO)₉] in toluene the iron tetracarbonyl complex **1** is formed in moderate yield (59%) (Scheme 1). In this yellow complex, the iron tetracarbonyl fragment is coordinated by the bridging phosphorus atom P⁹. The formation of **1** does not succeed in THF but only in toluene, and an excess of metal complex precursor (two equivalents) is required to obtain a satisfying yield. Although compound **1** is formed in toluene, dissociation in toluene (approximately 10 mol%) is observed in the ³¹P{¹H} NMR spectrum, while no dissociation occurs in THF.

^aUniversität Leipzig, Fakultät für Chemie und Mineralogie, Institut für Anorganische Chemie, Johannisallee 29, 04103 Leipzig, Germany. E-mail: hey@uni-leipzig.de

^bDipartimento di Chimica, Università degli Studi di Milano, Via Camillo Golgi 19, 20131 Milano, Italy

† Electronic supplementary information (ESI) available. CCDC 2144600–2144604. For ESI and crystallographic data in CIF or other electronic format see DOI: <https://doi.org/10.1039/d2dt01691e>



Scheme 1 Reaction of nonaphospane **L** to form the metal complexes **1–5** ([Fe] = Fe(CO)₄, [Co] = Co(CO)₂(NO), [Cu] = CuBr, [Rh] = Rh(CO)Cl, [Pd] = PdCl₂, COD = cycloocta-1,5-diene).

The iron(0) complex **1** crystallises in the monoclinic space group *I2/a* with four molecules per unit cell (Fig. 1). While the bond angle Fe1–C20–O4 (*trans* orientation with respect to the Fe–P bond) is almost 180°, the Fe–C–O bond angles of the carbonyl groups in the trigonal plane deviate slightly from a linear arrangement (Fe1–C17–O1 172.6(6)°, Fe1–C18–O2 173.7(6)°, Fe1–C19–O3 169.0(1)°). This can be explained by the space demand of the ligand **L** forcing the carbonyl ligands out of their ideal positions. As the asymmetric molecule is located

on a twofold axis, the *tert*-butyl and {Fe(CO)₄} substituents on P9 are disordered for symmetry reasons. Thus, the substituents overlap to a certain extent and impede a precise bond parameter analysis. This also applies to the Fe1–P9 bond length (236.4(1) pm) which is slightly larger than in comparable compounds (around 228 pm).^{37–39}

DFT calculations (DFT-D4//TPSSH/ZORA-def2-TZVP) show that the difference in Gibbs free energy for the formation of **1** with 0.5 equivalents [Fe₂(CO)₉] as metal precursor with loss of half an equivalent of carbon monoxide is exergonic with –40.6 kJ mol^{–1} (Scheme S1, ESI[†]). Further loss of carbon monoxide in **1** to furnish a chelate complex [Fe(CO)₃(L-κ²P⁶,P⁹)] is energetically unfavoured (Δ*G* = +32.6 kJ mol^{–1}), and consequently, the formation of **1** as {Fe(CO)₄} complex is the only energetically feasible complexation reaction.

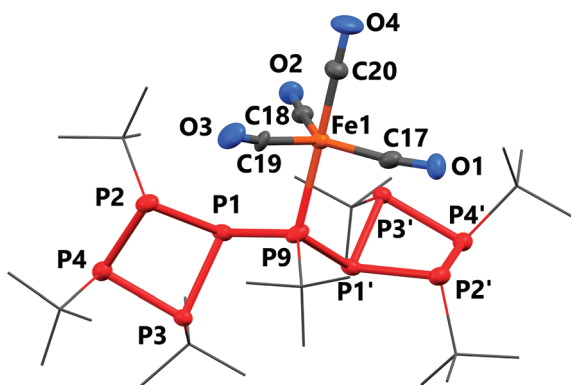


Fig. 1 Molecular structure of **1**. Hydrogen atoms and the disorder over the twofold axis are omitted and *tert*-butyl groups are drawn as wire-frames for clarity. Thermal ellipsoids are shown at 50% probability level. The labels of the phosphorus atoms P⁵–P⁸ (P1'–P4') refer to their respective symmetry equivalent atoms. Selected bond lengths [pm] and angles [°]: Fe1–C17 179.1(7), Fe1–C18 179.6(7), Fe1–C19 182.0(1), Fe1–C20 178.8(6), C17–O1 115.5(8), C18–O2 114.6(7), C19–O3 112.0(1), C20–O4 114.2(7), Fe1–P9 236.4(1), P9–Fe1–C17 92.1(2), P9–Fe1–C18 91.9(2), P9–Fe1–C19 89.2(5), P9–Fe1–C20 178.8(2), Fe1–C17–O1 172.6(6), Fe1–C18–O2 173.7(6), Fe1–C19–O3 169.0(1), Fe1–C20–O4 179.5(7), P1–P9–P1' 90.42(5).

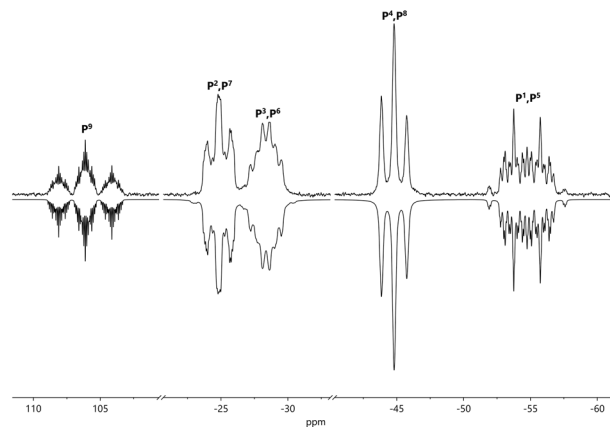


Fig. 2 Experimental (top) and simulated (bottom) ³¹P{¹H} NMR spectrum of **1** at 162 MHz in THF-*d*⁸ (*R* = 0.22%).

Table 1 $^{31}\text{P}\{^1\text{H}\}$ NMR parameters of **1** at 162 MHz in THF- d^8 at 25 °C ([AMNR] $_2$ X spin system, C_s symmetrisation, $R = 0.22\%$)

δ/ppm	J_{PP}/Hz	J_{PP}/Hz (interannular)	H/Hz
$\delta_1 = \delta_5 = -54.72$	$J_{1,2} = J_{5,7} = -168.1(1)$	$J_{1,5} = +192.1(2)$	$H_1 = H_5 = 11.4(1)$
$\delta_2 = \delta_7 = -24.86$	$J_{1,3} = J_{5,6} = -161.9(1)$	$J_{1,6} = J_{3,5} = +2.1(1)$	$H_2 = H_7 = 16.0(2)$
$\delta_3 = \delta_6 = -28.39$	$J_{1,4} = J_{5,8} = +22.8(1)$	$J_{1,7} = J_{2,5} = +5.4(1)$	$H_3 = H_6 = 28.2(3)$
$\delta_4 = \delta_8 = -44.79$	$J_{2,3} = J_{6,7} = +19.2(1)$	$J_{1,8} = J_{4,5} = 0.0(1)$	$H_4 = H_8 = 25.0(1)$
$\delta_9 = 106.10$	$J_{2,4} = J_{7,8} = -156.64(4)$	$J_{1,9} = J_{5,9} = -321.93(3)$	$H_9 = 5.60(4)$
	$J_{3,4} = J_{6,8} = -150.20(4)$	$J_{2,6} = J_{3,7} = +2.1(3)$	
		$J_{2,7} = -2.5(4)$	
		$J_{2,8} = J_{4,7} = -0.7(3)$	
		$J_{2,9} = J_{7,9} = +34.82(3)$	
		$J_{3,6} = +5.72(6)$	
		$J_{3,8} = J_{4,6} = +2.7(7)$	
		$J_{3,9} = J_{6,9} = +78.39(3)$	
		$J_{4,8} = 0(2)$	
		$J_{4,9} = J_{8,9} = +16.14(4)$	

δ , chemical shift; J , coupling constant; H , spectral half width.

As expected, four stretching vibrations of the CO ligands are observed in the IR spectrum. The $^{31}\text{P}\{^1\text{H}\}$ NMR spectrum of compound **1** is governed by an [AMNR] $_2$ X spin system (Fig. 2). The corresponding parameters were successfully determined by automated line-shape analysis (Table 1). The most striking features are — apart from considerable line broadening — the rather large $^1J_{\text{PP}}$ coupling $J_{1,9}/J_{5,9}$ ($-321.93(3)$ Hz) and the $^2J_{\text{PP}}$ coupling $J_{1,5}$ ($+192.1(2)$ Hz). The magnitude of the latter is larger than in $\{\text{cyclo}-(\text{P}^t\text{Bu}_3)\}_2\text{CH}_2$ ($+164.03$ Hz),³⁶ an [A[M] $_2$ X] $_2$ spin system,[‡] but comparable to exocyclic 2J couplings in similar compounds.^{40,41} This large magnitude indicates that the respective lone pairs of electrons point towards each other. Therefore, the conformation in solution differs from that observed in the solid state which thus indicates a free rotation around the P⁹–P¹ and P⁹–P⁵ bonds (P⁹–P¹ and P⁹–P^{1'}, respectively, in Fig. 1). The couplings within the four-membered rings have values which are similar to those of related *tert*-butyl substituted cyclotetraphosphanes.[§]^{29,36,42}

‡ The most commonly used nomenclature to designate spin systems was first proposed by Pople, Schneider and Bernstein⁴³ and later extended by Richards and Schaefer.⁴⁴ As this nomenclature becomes very cumbersome for complex spin systems, Haigh proposed a more condensed nomenclature, involving the use of square brackets to indicate repeated symmetry-related magnetically non-equivalent groups of nuclei with all nuclei within the square brackets to be magnetically equivalent.⁴⁵ Thus, for example the spin system of **3** which is observed in the $^{31}\text{P}\{^1\text{H}\}$ NMR spectrum at room temperature could be either designated as an AA'MM'M'M'RR'X or an [A[M] $_2$ R] $_2$ X spin system. However, as the latter notation is very uncommon (likely due to the circumstance that it is rarely needed since highly symmetrical, strongly coupled spin systems are mainly observed in oligophosphanes) and might be inconclusive for the reader, in our previous work,³⁶ we used a 'hybrid' notation in the style of [AMM'X] $_2$ to signify the spin system's nature as two AM $_2$ X spin systems connected to each other, allowing the observation of the MM' couplings. To avoid confusion, here, we refer to the nomenclature of Haigh.

§ J. B. Robert, A. Cogne *et al.* reported a $^1J_{\text{PP}}$ coupling of 148.4 Hz in $\text{cyclo}-(\text{P}^t\text{Bu})_4$.⁴² Unlike than stated in some textbooks,⁴⁶ they assumed the absolute sign to be negative.

[Co(CO) $_2$ (NO)]($\{\text{cyclo}-(\text{P}^t\text{Bu}_3)\}_2\text{P}^t\text{Bu}-\kappa\text{P}^9$) (**2**)

The reaction of nonaphosphane **L** and a threefold excess of cobalt tricarbonyl nitrosyl ([Co(CO) $_3$ (NO)]) in THF at 60 °C gives the cobalt dicarbonyl nitrosyl phosphane complex **2** in good yield (79%) (Scheme 1). If the reaction is conducted with only one equivalent of metal complex precursor, conversion is incomplete even after several days of heating (followed by $^{31}\text{P}\{^1\text{H}\}$ NMR spectroscopy). With at least two equivalents, clean conversion is observed, but a rapid workup is necessary as the rust red complex **2** decomposes in solution when no [Co(CO) $_3$ (NO)] is present. Decomposition is fast in apolar or less polar solvents, such as alkanes, benzene or toluene. In THF, **2** is more stable, but decomposition is also observed within days to weeks. In every case, decomposition leads to formation of the free ligand suggesting that the Co–P bond is apparently labile. However, **2** is stable as a solid under inert gas at -30 °C.

In contrast to octaphosphane $\{\text{cyclo}-(\text{P}^t\text{Bu}_3)\}_2$,²⁹ the nonaphosphane does not form the corresponding cobalt monocarbonyl nitrosyl complex in which the ligand coordinates in a bidentate bonding mode. DFT calculations (DFT-D4//TPSSH/ZORAdef2-TZVP) showed that this reaction is in fact energetically unfavoured (Scheme S1, ESI[†]). The formation of [Co(CO) $_2$ (NO)(L- κP^9)] (**2**) is slightly exergonic ($\Delta G = -7.5$ kJ mol $^{-1}$), but further release of carbon monoxide is endergonic with $\Delta G = +49.3$ kJ mol $^{-1}$. Conversely, for the corresponding $\{\text{cyclo}-(\text{P}^t\text{Bu}_3)\}_2$ complex, ΔG is slightly endergonic ($+9.2$ kJ mol $^{-1}$) for the release of the first CO, but exergonic for loss of the second CO ligand (-5.6 kJ mol $^{-1}$) resulting in an overall reaction energy of $+3.6$ kJ mol $^{-1}$, low enough to overcome the energy barrier when taking the continuous removal of gaseous CO from the system into account.²⁹

Single crystals of **2** were obtained from *n*-pentane at -30 °C. The complex crystallises in the triclinic space group $P\bar{1}$ with two symmetry-independent molecules in the asymmetric unit with cobalt being coordinated in a tetrahedral fashion (Fig. 3). The Co–P bond (226.0(1) pm, 227.19(9) pm) is

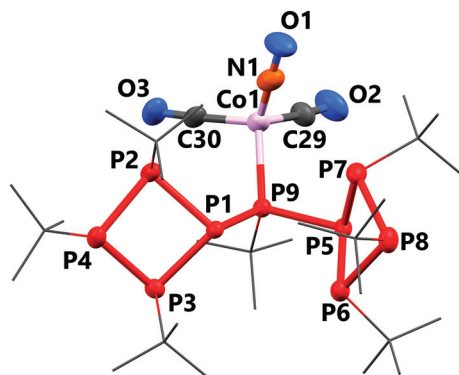


Fig. 3 Molecular structure of **2**. Only one of the two symmetry-independent molecules is shown. Hydrogen atoms are omitted and *tert*-butyl groups are drawn as wireframes for clarity. Thermal ellipsoids are shown at 50% probability level. Selected bond lengths [pm] and angles [°] (parameters of the second symmetry-independent molecule are given in square brackets): Co1–P9 226.0(1) [227.19(9)], Co1–N1 167.0(4) [169.1(3)], Co1–C29 175.2(4) [175.7(4)], Co1–C30 176.5(4) [176.8(4)], N1–O1 118.1(4) [116.7(4)], C29–O2 114.5(4) [114.4(4)], C30–O3 114.1(4) [114.4(4)], P9–Co1–C29 103.6(1) [105.2(1)], P9–Co1–C30 100.8(1) [102.2(1)], P9–Co1–N1 118.7(1) [118.5(1)], Co1–C29–O2 174.9(4) [174.0(4)], Co1–C30–O3 176.9(3) [174.3(3)], Co1–N1–O1 169.5(3) [170.8(3)], P1–P9–P5 104.45(5) [104.90(4)].

slightly longer than in related cobalt dicarbonyl nitrosyl phosphane complexes (around 222 pm).^{47–49} All bond angles involving cobalt and nitrogen are larger (110.2(2)°–118.7(1)°) while those involving carbon instead of nitrogen are smaller (100.8(1)°–108.5(2)°) than in an ideal tetrahedron (109.47°).

In the IR spectrum of **2**, two CO and one NO stretching vibrations are observed. X-ray diffraction studies and the IR spectrum confirm an almost linear coordination of the nitrosyl ligand (Co1–N1–O1 169.5(3)° [170.8(3)°]) to the cobalt atom which is in accordance with similar compounds.²⁹ The ³¹P{¹H} NMR spectrum of **2** (Fig. 4) is comparable to that of **1** as both constitute an [AMNR]₂X spin system. The full parameter set was determined by automated line-shape analysis (Table 2).

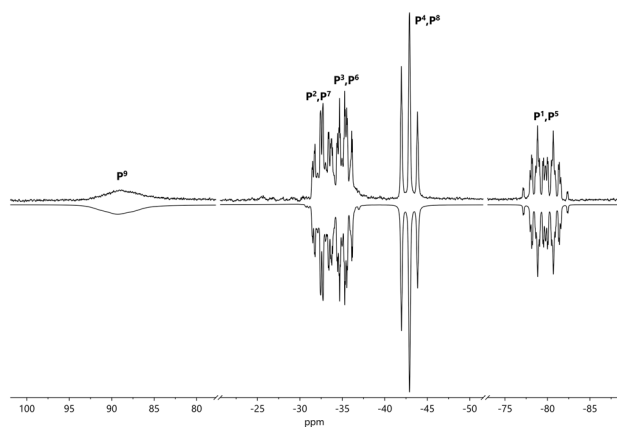
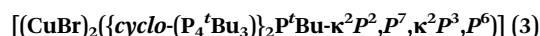


Fig. 4 Experimental (top) and simulated (bottom) ³¹P{¹H} NMR spectrum of **2** at 162 MHz in THF-*d*⁸ (*R* = 0.55%).

The [AMNR]₂ part looks similar to the one observed for **1**, but the X part (P⁹) appears as a very broad singlet (line broadening *H*₉ = 352(7) Hz), caused by the quadrupolar nucleus ⁵⁹Co (*I* = 7/2, NA = 100%), as was also observed in comparable compounds (e.g., [Co(NO)(CO){*cyclo*-(P⁴Bu₃)₂-κ²P²,P⁴}]²⁹). As the NMR spectra do not indicate the presence of a paramagnetic moiety, cobalt has retained its d¹⁰ configuration (oxidation state –I) in the complex. The magnitude of the ²*J*_{PP} coupling constant *J*_{1,5} (+163.8(1) Hz) is still large, even though smaller than in **1**, again indicating a different conformation of the complex in solution than the one observed in the solid state.

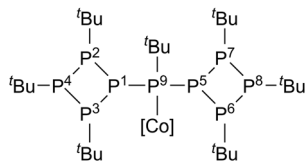


Complexation of two {CuBr} fragments yielding a dinuclear complex was achieved by reaction of **L** with two equivalents of [CuBr(SME₂)] in THF (79% yield). Unlike {*cyclo*-(P⁴Bu₃)₂},²⁹ nonaphospane **L** does not form a mononuclear copper(i) complex. Less than two equivalents of [CuBr(SME₂)] just lead to the observation of mixtures of **3** and **L** according to the ³¹P{¹H} NMR spectrum. DFT calculations confirmed that the reaction of two hypothetical molecules of the respective mononuclear copper(i) complex to form one molecule **L** and one molecule **3** is in fact exergonic by –1.3 kJ mol^{–1} (Scheme S3, ESI†). The dinuclear complex **3** crystallises with one non-coordinating THF molecule in the monoclinic space group *P*₂₁/*c* (Fig. 5). The P1–P9–P5 bond angle (118.40(4)°) involving the bridging phosphorus atom is larger in comparison to the free ligand **L** (106.83(1)°),³⁶ **1** (90.42(5)°) or **2** (104.45(5)°). The deformation is caused by the coordination of two copper atoms in a bidentate bonding mode. A similar adjustment has been observed for monometallic complexes of {*cyclo*-(P⁴Bu₃)₂}, where the angles involving the exocyclic P–P bonds are increased (accompanied by shorter P–P bond lengths between the rings) compared to the free ligand.²⁹ The Cu–P bond lengths (224.44(5) to 224.73(5) pm) are similar to those in the corresponding octaphospane complex [(CuBr)₂{(*cyclo*-(P⁴Bu₃)₂-κ²P²,P²,κ²P⁴,P⁴)] (225.01(6) pm),²⁹ but the copper atoms in **3** have an almost ideal trigonal-planar coordination sphere with bond angles close to 120° (117.64(2)°–121.72(2)°), suggesting that nonaphospane **L** is indeed more flexible than the octaphospane {*cyclo*-(P⁴Bu₃)₂}. The *tert*-butyl-P⁹ fragment is disordered either facing Cu1 or Cu2 (ratio 0.563(2) : 0.437(2)).

At room temperature, in the ³¹P{¹H} NMR spectrum of **3**, an [A[M]₂R]₂X spin system is observed (Fig. 6). The ³¹P{¹H} NMR parameters were determined by automated line-shape analysis (Table 3). The resonance of the phosphorus atoms which are coordinating at the copper atoms (*δ*₂, *δ*₃, *δ*₆, *δ*₇) is broadened due to the quadrupole moment of the copper nuclei ⁶³Cu (*I* = 3/2, NA = 69.17%) and ⁶⁵Cu (*I* = 3/2, NA = 30.83%). Caused by their fast relaxation, no ³¹P–^{63/65}Cu coupling can be observed. The large magnitude of the ¹*J*_{PP} coupling *J*_{1,9}/*J*_{5,9} (–451.21(2) Hz) is remarkable and probably due to complexation forcing the ligand into a strained conformation. This affects also the intraannular as well as the interannular ²*J*_{PP} couplings with the former displaying large values. The large

Table 2 $^{31}\text{P}\{^1\text{H}\}$ NMR parameters of **2** at 162 MHz in THF- d^8 at 25 °C ([AMNR] $_2$ X spin system, C_s symmetrisation, $R = 0.55\%$)

δ/ppm	J_{PP}/Hz	J_{PP}/Hz (interannular)	H/Hz
$\delta_1 = \delta_5 = -79.77$	$J_{1,2} = J_{5,7} = -162.7(1)$	$J_{1,5} = +163.8(1)$	$H_1 = H_5 = 13.2(1)$
$\delta_2 = \delta_7 = -32.60$	$J_{1,3} = J_{5,6} = -149.7(1)$	$J_{1,6} = J_{3,5} = +13.8(1)$	$H_2 = H_7 = 14.1(1)$
$\delta_3 = \delta_6 = -35.02$	$J_{1,4} = J_{5,8} = +17.9(1)$	$J_{1,7} = J_{2,5} = +11.1(1)$	$H_3 = H_6 = 11.6(1)$
$\delta_4 = \delta_8 = -42.87$	$J_{2,3} = J_{6,7} = +15.8(1)$	$J_{1,8} = J_{4,5} = -1.9(3)$	$H_4 = H_8 = 18.1(1)$
$\delta_9 = 89.41$	$J_{2,4} = J_{7,8} = -157.6(1)$	$J_{1,9} = J_{5,9} = -300.0(1)$	$H_9 = 352(7)$
	$J_{3,4} = J_{6,8} = -150.32(2)$	$J_{2,6} = J_{3,7} = +2.9(2)$	
		$J_{2,7} = +1.1(4)$	
		$J_{2,8} = J_{4,7} = +1.3(3)$	
		$J_{2,9} = J_{7,9} = +45.4(1)$	
		$J_{3,6} = +0.04(2)$	
		$J_{3,8} = J_{4,6} = +1.1(2)$	
		$J_{3,9} = J_{6,9} = +94.9(1)$	
		$J_{4,8} = 0.0(3)$	
		$J_{4,9} = J_{8,9} = -15.1(1)$	



δ , chemical shift; J , coupling constant; H , spectral half width.

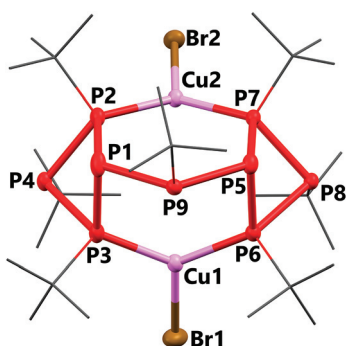


Fig. 5 Molecular structure of **3**. Hydrogen atoms, solvent molecules and disorder of the *tert*-butyl- P^9 fragment are omitted and *tert*-butyl groups are drawn as wireframes for clarity. Thermal ellipsoids are shown at 50% probability level. Selected bond lengths [pm] and angles [°]: Cu1–Br1 232.99(3), Cu2–Br2 234.43(3), Cu1–P3 224.54(6), Cu1–P6 224.73(5), Cu2–P2 224.59(5), Cu2–P7 224.44(5), P3–Cu1–P6 121.72(2), P2–Cu2–P7 120.95(2), P3–Cu1–Br1 118.40(2), P6–Cu1–Br1 119.01(2), P2–Cu2–Br2 117.64(2), P7–Cu2–Br2 119.73(2), P1–P9–P5 118.40(4).

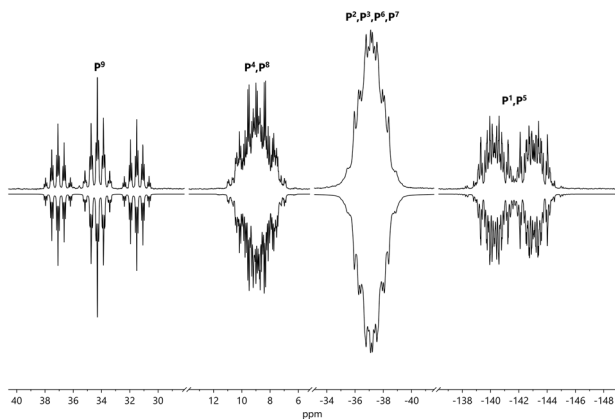


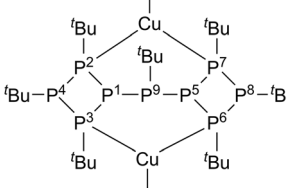
Fig. 6 Experimental (top) and simulated (bottom) $^{31}\text{P}\{^1\text{H}\}$ NMR spectrum of **3** at 162 MHz in benzene- d^6 ($R = 0.41\%$).

$^2J_{\text{PP}}$ coupling $J_{2,7}/J_{3,6}$ (134.8(1) Hz) can be explained by coupling *via* the copper atom. Large $^2J_{\text{PP}}$ couplings were also observed in the corresponding rhodium complex of the octa-phosphane and other cyclophosphanes with exocyclic P–P bonds.^{29,40,41} In complexes **1–3**, there seems to be a relationship between the $^2J_{\text{PP}}$ coupling $J_{1,5}$ and the P–P–P bond angle involving the bridging phosphorus atom P^9 . Smaller bond angles (P2–P9–P2', 90.42(5)° in **1**; P1–P9–P5, 104.45(5)° in **2**) result in a larger magnitude of the coupling constant (192.1(2) Hz (**1**), 163.8(1) Hz (**2**)), whereas a larger bond angle (P1–P9–P5, 118.40(4)° in **3**) leads to a smaller $J_{1,5}$ value (55.6(1) Hz).

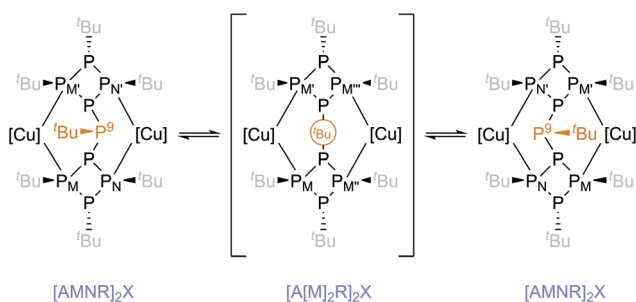
The observation of an $[\text{A}[\text{M}]\text{R}]_2\text{X}$ spin system is in contradiction to the expectation that arises from the solid-state structure. Since the *tert*-butyl group at P^9 is facing one of the copper atoms, actually an $[\text{AMNR}]_2\text{X}$ spin system is expected in the $^{31}\text{P}\{^1\text{H}\}$ NMR spectrum of **3**, too. However, this experimental finding can be explained by a flip of the *tert*-butyl- P^9 fragment which involves an inversion at the phosphorus atom (P^9). This leads to C_{2v} symmetry in solution on the NMR time scale (Scheme 2) and the observation of this highest possible symmetry among the observable conformations.⁵⁰ Thus, there are two equivalent conformers with C_s symmetry converting into each other *via* a C_{2v} symmetric transition state for which we calculated an activation barrier of +45.3 kJ mol⁻¹ (DFT-D4//TPSSH/ZORA-def2-TZVP).

Indeed, in the ^1H NMR spectrum of **3**, a broad doublet with the largest integral can be assigned to the *tert*-butyl protons of the groups attached to P^2 , P^3 , P^6 and P^7 which is consistent with C_{2v} symmetry and line broadening caused by the quadrupole moment of the copper nuclei. In the $^1\text{H}\{^{31}\text{P}\}$ NMR spectrum, this resonance consequently appears as a broad singlet. If flipping of the *tert*-butyl group at P^9 is hindered (Scheme 2), the point group of the molecule changes to C_s resulting in the appearance of a second resonance, as P^2 and P^3 (and P^6 and P^7 , respectively) and the attached *tert*-butyl groups become chemically non-equivalent (in this case, an $[\text{AMNR}]_2\text{X}$ spin

Table 3 $^{31}\text{P}\{^1\text{H}\}$ NMR parameters of **3** at 162 MHz in benzene- d^6 at 25 °C ($[\text{A}[\text{M}]_2\text{R}]_2\text{X}$ spin system, C_{2v} symmetrisation, $R = 0.41\%$)

δ/ppm	J_{PP}/Hz	J_{PP}/Hz (interannular)	H/Hz
$\delta_1 = \delta_5 = -141.66$	$J_{1,2} = J_{1,3} = J_{5,6} = J_{5,7} = -141.62(4)$	$J_{1,5} = +55.6(1)$	$H_1 = H_5 = 6.05(4)$
$\delta_2 = \delta_3 = \delta_6 = \delta_7 = -37.17$	$J_{1,4} = J_{5,8} = +94.76(4)$	$J_{1,6} = J_{1,7} = J_{2,5} = J_{3,5} = +6.59(3)$	$H_2 = H_3 = H_6 = H_7 = 23.5(1)$
$\delta_4 = \delta_8 = 8.94$	$J_{2,3} = J_{6,7} = +39.9(1)$	$J_{1,8} = J_{4,5} = +0.67(4)$	$H_4 = H_8 = 5.96(4)$
$\delta_9 = 34.27$	$J_{2,4} = J_{3,4} = J_{6,8} = J_{7,8} = -187.10(3)$	$J_{1,9} = J_{5,9} = -451.21(2)$	$H_9 = 5.24(3)$
		$J_{2,6} = J_{3,7} = +1.00(4)$	
		$J_{2,7} = J_{3,6} = +134.8(1)$	
		$J_{2,8} = J_{3,8} = J_{4,6} = J_{4,7} = -1.21(4)$	
		$J_{2,9} = J_{3,9} = J_{6,9} = J_{7,9} = +70.90(2)$	
		$J_{4,8} = -3.6(1)$	
		$J_{4,9} = J_{8,9} = -14.87(2)$	

δ , chemical shift; J , coupling constant; H , spectral half width.



Scheme 2 Visualisation of the $\{tert\text{-butyl-P}^9\}$ flip in complex **3** with the corresponding spin system denoted in lilac. The molecule with the highest symmetry (C_{2v}) corresponds to the transition state ($\Delta G_{\text{act}} = +45.3 \text{ kJ mol}^{-1}$) which is observed as averaged structure in solution. Hampering the flip of the $tert\text{-butyl}$ group by cooling leads to observation of the conformation (minimum energy structure) with C_s symmetry in the NMR spectrum. The orange circle represents the phosphorus atom P^9 eclipsed by the $tert\text{-butyl}$ group ($[\text{Cu}] = \{\text{CuBr}\}$).

system, comparable to **1** and **2**, would be observed in the $^{31}\text{P}\{^1\text{H}\}$ NMR spectrum). In fact, VT $^1\text{H}\{^{31}\text{P}\}$ NMR experiments (Fig. S15, ESI †) show coalescence of both resonances at $-58.1 \text{ }^\circ\text{C} \pm 1 \text{ }^\circ\text{C}$. With this experimental result, an energy barrier of $+45.4 \text{ kJ mol}^{-1}$ was determined for the $\{tert\text{-butyl-P}^9\}$ flip which is in excellent agreement with the theoretical value of $+45.3 \text{ kJ mol}^{-1}$.

$[\text{RhCl}(\text{CO})\{\{\text{cyclo}(\text{P}_4\text{Bu}_3)\}_2\text{P}^t\text{Bu-}\kappa^2\text{P}^6, \text{P}^9\}]$ (**4**)

The rhodium complex $[\{\text{RhCl}(\text{CO})\}_2]$ reacts with **L** in THF with release of carbon monoxide (Scheme 1). The reaction proceeds within minutes, furnishing the intense orange complex $[\text{RhCl}(\text{CO})\{\{\text{cyclo}(\text{P}_4\text{Bu}_3)\}_2\text{P}^t\text{Bu-}\kappa^2\text{P}^6, \text{P}^9\}]$ (**4**) in good yield (86%) after workup. Compound **4** crystallises in the monoclinic space group $\text{P}2_1/c$ with four molecules per unit cell (Fig. 7). Due to the *trans* effect, caused by the carbonyl ligand at the rhodium atom, the Rh1–P6 bond length (235.62(5) pm) is considerably larger than the Rh1–P9 bond length (221.91(5) pm), but the bond lengths are similar to those of the respective octaphosphaane rhodium(i) complex.²⁹

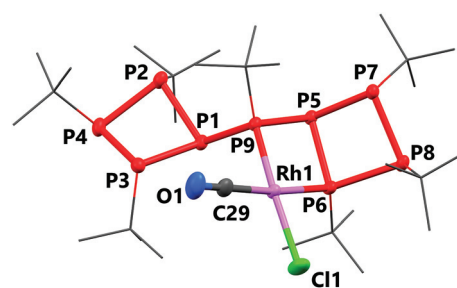


Fig. 7 Molecular structure of **4**. Hydrogen atoms are omitted and *tert*-butyl groups are drawn as wireframes for clarity. Thermal ellipsoids are shown at 50% probability level. Selected bond lengths [pm] and angles [$^\circ$]: Rh1–C29 188.7(2), C29–O1 110.9(3), Rh1–Cl1 236.53(6), Rh1–P6 235.62(5), Rh1–P9 221.91(5), P1–P2 222.49(7), P5–P6 222.42(7), P6–P8 220.54(7), C29–Rh1–Cl1 93.71(7), P6–Rh1–P9 78.84(2), P1–P9–P5 92.63(3), P1–P2–P4 84.70(3), P5–P6–P8 89.50(3), P6–P5–P9 81.34(2).

As all phosphorus atoms of compound **4** are magnetically non-equivalent, the ABCDEFGHIJ portion of an ABCDEFGHIJX spin system (with ^{103}Rh ($I = 1/2$, $\text{NA} = 100\%$) as nucleus X) is observed in the $^{31}\text{P}\{^1\text{H}\}$ NMR spectrum, which displays nine resonances with equal integrals. Due to strong line-broadening effects, line-shape analysis did not lead to satisfying results. Unlike $[\text{RhCl}(\text{CO})\{\{\text{cyclo}(\text{P}_4\text{Bu}_3)\}_2\text{-}\kappa^2\text{P}^2, \text{P}^4\}]$,²⁹ there are no resonances shifted strongly to low field. Besides the signals which can be attributed to the ABCDEFGHIJX spin system, further signals with a weaker intensity are detectable in the $^{31}\text{P}\{^1\text{H}\}$ NMR spectrum (Fig. S24, ESI †). When single crystals of **4** are dissolved, the same NMR spectrum as for the bulk material is observed. This indicates that these additional signals correspond to one or more compounds which are formed from complex **4** in solution. In fact, in contrast to complexes **1–3**, the asymmetric molecular structure of the complex would allow the formation of several non-equivalent configurational isomers, resulting in additional signals in the solution NMR spectra. Different isomers could indeed be observed for platinum(ii) complexes of the octaphosphaane $\{\text{cyclo}(\text{P}_4\text{Bu}_3)\}_2$ as well as for the respective gold(i) complexes, which moreover

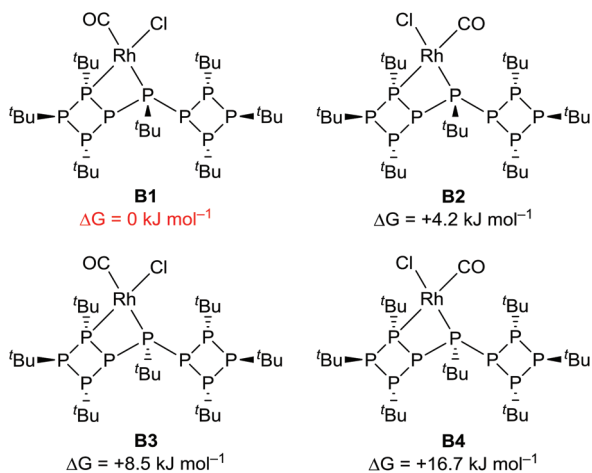


Fig. 8 Low energy configurational isomers **B1**–**B4** of the rhodium(*i*) complex **4**. Minimum energy labelled in red.

showed a rapid interconversion.^{29,51} To investigate this possibility for complex **4**, DFT calculations of different conceivable configurational isomers were conducted to access their relative energies (Scheme S2, ESI[†]). Fig. 8 shows the structural formulas of four out of the eight possible configurational isomers, together with their relative Gibbs energy. Configuration **B1** corresponds to the one observed in the solid state. Obviously, configurational isomers with six-membered chelate rings (**B5**–**B7**, Scheme S2, ESI[†]) are energetically unfavoured and are thus less likely to be formed in solution. However, configurational isomers **B2**–**B4** (Fig. 8) with four-membered chelate rings have a similar relative energy. Isomer **B2** for instance (formal exchange of CO and Cl co-ligands) has a relative energy of only +4.2 kJ mol⁻¹ and, assuming an equilibrium in solution, could thus be the species observed in the NMR spectrum. The activation energy for the transformations between the different isomers was not calculated, but it is reasonable to assume that they are low enough to proceed at room temperature considering the transformation reactions of oligophosphane complexes observed for similar systems.^{29,34,51}

Further complexation reactions

Attempts to prepare the corresponding complexes of nickel(0), palladium(II) or platinum(II) failed as either no complexation with **L** occurred ([Ni(COD)₂], COD = cycloocta-1,5-diene), the resulting complex decomposed ([PdCl₂(COD)]) or the ligand was degraded ([PtCl₂(COD)]). Apparently, the exocyclic P–P bonds between the *cyclo*-(P₄^tBu₃) rings and the bridging P^tBu moiety are activated by the coordinating metal, furnishing degradation products including *cyclo*-(P₄^tBu₃)P^tBuCl⁴⁰ or *cyclo*-(P₄^tBu₃)Cl⁵² (identified by ³¹P{¹H} NMR spectroscopy). While a few single crystals of the palladium(II) complex [PdCl₂({*cyclo*-(P₄^tBu₃)₂P^tBu-κ²P⁶,P⁹})] (**5**) could be obtained, due to decomposition it was not possible to reproduce this compound in larger quantities for further characterisation.

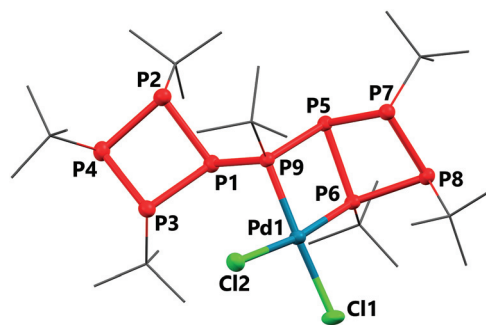


Fig. 9 Molecular structure of **5**. Hydrogen atoms are omitted and *tert*-butyl groups are drawn as wireframes for clarity. Thermal ellipsoids are shown at 50% probability level. Selected bond lengths [pm] and angles [°]: Pd1–P9 223.2(1), Pd1–P6 225.5(1), Pd1–Cl1 235.1(1), Pd1–Cl2 234.1(1), P6–Pd1–P9 80.08(4), P9–Pd1–Cl2 91.42(4), P9–Pd1–Cl1 172.70(4), Cl2–Pd9–Cl1 94.90(4), P1–P9–P5 93.69(6), P6–P5–P9 80.71(6).

Compound **5** essentially shows the same structural parameters as the rhodium complex **4** (Fig. 9).

Comparative analysis

The configurational isomers of the bidentate rhodium complex **4** led us to investigate the different bonding modes of the monodentate complexes **1** and **2**. In these complexes, only one phosphorus atom coordinates at the metal atom resulting in four possible constitutional isomers according to the four different types of phosphorus atoms in the nonaphosphane. The different constitutions for both iron(0) (**1**) and cobalt(–I) (**2**) complexes are shown in Scheme S4 (ESI[†]) together with their relative energies. The coordination of the bridging phosphorus atom P⁹ (**M1**, Scheme S4, ESI[†]), corresponding to the constitution observed in the experiment, is energetically most favoured. All other constitutions have a considerably higher relative energy in contrast to the isomers with bidentate bonding mode as in case of complex **4** with energies close to the most stable structures. As observed for complexes of the octaphosphane {*cyclo*-(P₄^tBu₃)₂}, coordination of the phosphorus atom with no attached *tert*-butyl groups is energetically much less favoured (**M2**, Scheme S4, ESI[†]).²⁹

The formal insertion of the central P^tBu group in **L** enables the monodentate bonding mode observed for **1** and **2** in addition to the different monometallic and bimetallic chelate bonding modes that have been observed for {*cyclo*-(P₄^tBu₃)₂}.²⁹ To get further insight into the differences between both ligands, we compared the complex formation energies of complexes **3** and **4** and the analogous complexes with {*cyclo*-(P₄^tBu₃)₂} (Scheme S5, ESI[†]). In both cases, the formation energy is significantly higher for nonaphosphane **L** (12.4 kJ mol⁻¹ for {RhCl(CO)} and 17.4 kJ mol⁻¹ for 2 {CuBr}). This indicates a better accommodation of the metal fragments and thus a higher flexibility of **L** compared to {*cyclo*-(P₄^tBu₃)₂}.

Thermolysis

Metal complexes of cyclooligophosphanes can be potential precursors for the preparation of phosphorus-rich metal

phosphides.^{29,53,54} However, thermolysis up to 380 °C of compounds **1–4** (Fig. S2–S5, ESI†) resulted in amorphous products (powder X-ray diffraction studies) without clear stoichiometric compositions as deduced from the mass losses.

Conclusions

The nonaphosphane $\{\text{cyclo}-(\text{P}_4^t\text{Bu}_3)\}_2\text{P}^t\text{Bu}$ (**L**) displays a coordination chemistry different from the related octaphosphane $\{\text{cyclo}-(\text{P}_4^t\text{Bu}_3)\}_2$ due to the more flexible phosphorus scaffold, as corroborated also by quantum chemical calculations. Transition metal complexes with iron(0) ($[\text{Fe}(\text{CO})_4\text{L}]$ (**1**)), cobalt(–I) ($[\text{Co}(\text{CO})_2(\text{NO})\text{L}]$ (**2**)), copper(I) ($[\text{CuBr}_2\text{L}]$ (**3**)), rhodium(I) ($[\text{RhCl}(\text{CO})\text{L}]$ (**4**)) and palladium(II) ($[\text{PdCl}_2\text{L}]$ (**5**)) could be prepared and structurally characterised. The complex $^{31}\text{P}\{^1\text{H}\}$ NMR spectroscopic data of **1–3** were successfully determined by automated line-shape analysis allowing deeper insights into the relationship between structure and NMR spectroscopy.

Experimental

All manipulations were performed under nitrogen atmosphere using standard Schlenk techniques. Dry, oxygen-free solvents (THF, *n*-hexane, and toluene) were obtained from an MBraun Solvent Purification System MB SPS-800. Ethyl acetate (EtOAc, distilled from P_2O_5), THF (dynamic drying employing molecular sieve (3 Å)), and toluene were stored over molecular sieve (4 Å), *n*-hexane was stored over a potassium mirror. Solvents used for NMR spectroscopic measurements (benzene- d^6 , toluene- d^8 and THF- d^8) were distilled prior to use and stored over molecular sieve (4 Å). $[\text{CuBr}(\text{SMe}_2)]$,⁵⁵ $[\text{Fe}_2(\text{CO})_9]$,^{56,57} $[\text{RhCl}(\text{CO})_2]_2$,⁵⁸ $[\text{PdCl}_2(\text{COD})]^{59}$ (COD = cycloocta-1,5-diene) and $\{\text{cyclo}-(\text{P}_4^t\text{Bu}_3)\}_2\text{P}^t\text{Bu}^{36}$ (**L**) were prepared according to literature procedures. $[\text{Co}(\text{CO})_3(\text{NO})]$ was purchased from abcr (Karlsruhe). NMR spectra were recorded on a Bruker Avance III HD 400 MHz spectrometer at 25 °C. The coupling constants J are reported in hertz (Hz) and are absolute values if no sign is indicated. The chemical shift (δ) is given in ppm. ^1H NMR and ^{13}C NMR spectra were referenced either to SiMe_4 as internal standard or to the solvent residual signal. $^{31}\text{P}\{^1\text{H}\}$ NMR spectra were referenced using the Ξ scale⁶⁰ and recorded using 90° pulse angles and a D_1 time of 6.5 s. The temperature during $^1\text{H}\{^{31}\text{P}\}$ VT NMR experiments was determined with the aid of a methanol capillary inside the sample as internal standard.⁶¹ The activation energy of the *tert*-butyl- P^9 flip in complex **3** was calculated by using the approximation for uncoupled nuclei with equal intensity for the interconversion rate constant

$$k = \frac{\pi}{\sqrt{2}} \cdot \Delta\nu_{\text{AB}}$$

in combination with the Eyring equation which gave after rearranging

$$\Delta G = -RT_c \cdot \ln \left(\frac{\Delta\nu_{\text{AB}} h \pi}{k_{\text{B}} T_c \sqrt{2}} \right)$$

where ΔG is the activation energy in kJ mol^{-1} , T_c is the coalescence temperature in kelvin, $\Delta\nu_{\text{AB}}$ is the chemical shift difference of the fully resolved resonances before coalescence in hertz, k_{B} is the Boltzmann constant, R is the universal gas constant and h is the Planck constant.

Automated line-shape analysis of NMR spectra was done using Daisy under Bruker's TopSpin,⁶² assuming a negative relative sign for $^1J_{\text{PP}}$ coupling constants. Mass spectrometry was performed on a Bruker Daltonics Esquire 3000 Plus. TG/DSC analysis was done in Al_2O_3 crucibles on a Netzsch STA 449F1, with argon as protective gas and 5 K min^{-1} heating rate, heating up to 350–380 °C. IR spectra were recorded on a Thermo Scientific Nicolet iS5 with a diamond ATR ($400\text{--}4000 \text{ cm}^{-1}$); for CHN analysis, a Heraeus Vario-EL oven was used.

Quantum chemical calculations were carried out with DFT using the programme ORCA⁶³ (version 5.0.1) with the convergence criterion set to tight SCF convergence and the atom-pairwise dispersion correction based on tight binding partial charges (D4).^{64,65} Relativistic effects were considered using Zero Order Regular Approximation (ZORA).⁶⁶ Furthermore, the RIJDX approximation was used to speed up the calculations, and in all cases, the free Gibbs energy ΔG was calculated using a numerical frequency analysis. The TPSSh functional^{67,68} in combination with the def2-TZVP⁶⁹ basis set showed the best agreement with the symmetric stretching vibration of the carbonyl moiety in complex **4** which was used as a benchmark (see Table S1, ESI†). The simulation of the solvent environment was performed using the conductor-like polarisable continuum model (C-PCM)⁷⁰ model. For calculations of all molecules, the solvent was set to be tetrahydrofuran.

Synthesis of $[\text{Fe}(\text{CO})_4(\{\text{cyclo}-(\text{P}_4^t\text{Bu}_3)\}_2\text{P}^t\text{Bu}-\text{kP}^9)]$ (**1**)

A suspension of 84.25 mg (0.124 mmol) **L** and 95.33 mg (0.262 mmol, 2.11 equiv.) $[\text{Fe}_2(\text{CO})_9]$ in 5 ml toluene was stirred for 15 h at ambient temperature. After filtration, the solvent was removed under reduced pressure and the obtained residue was washed four times with 2 ml EtOAc each until the washing liquid was colourless. The residue was dried at 60 °C *in vacuo*, furnishing 61.9 mg (0.073 mmol, 59%) of mustard yellow **1**. Brown-yellow crystals suitable for X-ray diffraction were obtained by recrystallisation in toluene.

Mp. loss of CO above 153 °C, further decomposition above 188 °C.

^1H NMR (400 MHz, THF- d^8): δ 1.78 (d, C_4H_9 , $^3J_{\text{HP}} = 15.7$ Hz, 9H), 1.35 (d, C_4H_9 , $^{2,3,6,7}J_{\text{HP}} = 12.9$ Hz, 36H), 1.27 (d, C_4H_9 , $^{4,8}J_{\text{HP}} = 13.0$ Hz, 18H) ppm.

$^{13}\text{C}\{^1\text{H}\}$ NMR (101 MHz, THF- d^8): δ 214.2 (d, $^2J_{\text{CP}} = 12.9$ Hz, CO), 47.4 (m, $\text{C}(\text{CH}_3)_3$, 9), 32.7 (m, $\text{C}(\text{CH}_3)_3$, 2,3,6,7), 31.3 (m, $\text{C}(\text{CH}_3)_3$, 9), 30.1 (m, $\text{C}(\text{CH}_3)_3$, 4,8), 28.5 (m, $\text{C}(\text{CH}_3)_3$, 2,3,4,6,7,8) ppm.

$^{13}\text{C}\{^1\text{H}, ^{31}\text{P}\}$ NMR (101 MHz, THF- d^8 , 28 °C): δ 214.2 (CO), 47.4 ($\text{C}(\text{CH}_3)_3$, 9), 32.8 ($\text{C}(\text{CH}_3)_3$, $^{2,7/3,6}$), 32.6 ($\text{C}(\text{CH}_3)_3$, $^{3,6/2,7}$), 31.1 ($\text{C}(\text{CH}_3)_3$, 9), 30.1 ($\text{C}(\text{CH}_3)_3$, 4,8), 28.6 ($\text{C}(\text{CH}_3)_3$, 4,8), 28.4 ($\text{C}(\text{CH}_3)_3$, $^{2,7/3,6}$), 28.3 ($\text{C}(\text{CH}_3)_3$, $^{3,6/2,7}$) ppm.

$^{31}\text{P}\{^1\text{H}\}$ NMR (162 MHz, THF- d^8): $[\text{A}[\text{M}]_2\text{R}]_2\text{X}$ spin system (C_s , $R = 0.22\%$, for full parameter set s. Table 1): δ 106.10

(m, P^9 , 1P), -24.86 (m, $P^{2,7}$, 2P), -28.39 (m, $P^{3,6}$, 2P), -44.79 (m, $P^{4,8}$, 2P), -54.72 (m, $P^{1,5}$, 2P) ppm.

IR: $\tilde{\nu}$ 2955 (m), 2936 (m), 2920 (m), 2889 (m), 2855 (m), 2036 (s, $\nu(\text{CO})$), 1963 (s, $\nu(\text{CO})$), 1929 (s, $\nu(\text{CO})$), 1904 (m, $\nu(\text{CO})$), 1584 (w), 1521 (w), 1468 (m), 1455 (m), 1389 (m), 1357 (m), 1168 (m), 1007 (w), 934 (w), 803 (m), 726 (w), 616 (s), 565 (w), 530 (s), 497 (m), 473 (m), 435 (w) cm^{-1} .

HR-ESI(+)-MS (THF): m/z 734.1912 $[\text{M} - 4\text{CO}]^+$, 762.1862 $[\text{M} - 3\text{CO}]^+$, 790.1813 $[\text{M} - 2\text{CO}]^+$, 818.1767 $[\text{M} - \text{CO}]^+$.

CHN, found: C, 45.41; H, 7.59; N, 0.00. $\text{C}_{32}\text{H}_{63}\text{FeO}_4\text{P}_9$ requires C, 45.41; H, 7.50; N, 0.00%.

Synthesis of $[\text{Co}(\text{CO})_2(\text{NO})\{\text{cyclo}-(\text{P}^4\text{Bu}_3)_2\text{P}^t\text{Bu}-\kappa\text{P}^9\}]$ (2)

A solution of 40 μl $[\text{Co}(\text{CO})_3(\text{NO})]$ in 1 ml THF (0.340 mmol, 2.9 equiv.) was added to 79.1 mg (0.117 mmol) **L** and heated to 60 °C for 20 h. After cooling to room temperature, all volatiles were removed *in vacuo*, yielding 99.3 mg crude **2**. The crude product was dissolved in 1.25 ml *n*-hexane; at -60 °C, a rust red precipitate formed. The mother liquor was decanted and the residue was dried at 60 °C *in vacuo*, furnishing **2** (75.7 mg, 0.092 mmol, 79%). Dark red single crystals suitable for X-ray diffraction were obtained by recrystallisation in *n*-pentane.

Mp. decomposition above 99 °C.

^1H NMR (400 MHz, THF- d^8): δ 1.59 (d, C_4H_9 , $^3J_{\text{HP}} = 15.9$ Hz, 9H), 1.33 (d, C_4H_9 , $^2,7/3,6/4,8$, $^3J_{\text{HP}} = 12.9$ Hz, 18H), 1.29 (d, C_4H_9 , $^2,7/3,6/4,8$, $^3J_{\text{HP}} = 12.7$ Hz, 18H), 1.25 (d, C_4H_9 , $^2,7/3,6/4,8$, $^3J_{\text{HP}} = 13.0$ Hz, 18H) ppm.

$^{13}\text{C}\{^1\text{H}\}$ NMR (101 MHz, THF- d^8): δ 44.2 (bs, $\text{C}(\text{CH}_3)_3$, 9), 33.9 (m, $\text{C}(\text{CH}_3)_3$, 2,3,6,7), 31.9 (bs, $\text{C}(\text{CH}_3)_3$, 9), 31.3 (m, $\text{C}(\text{CH}_3)_3$, 4,8), 29.8 (m, $\text{C}(\text{CH}_3)_3$, 2,3,4,6,7,8) ppm. The carbonyl signal could not be detected.

$^{13}\text{C}\{^1\text{H}, ^{31}\text{P}\}$ NMR (101 MHz, THF- d^8 , 28 °C): δ 44.2 ($\text{C}(\text{CH}_3)_3$, 9), 34.1 ($\text{C}(\text{CH}_3)_3$, $^{2,7/3,6}$), 33.7 ($\text{C}(\text{CH}_3)_3$, $^{3,6/2,7}$), 31.9 ($\text{C}(\text{CH}_3)_3$, 9), 31.3 ($\text{C}(\text{CH}_3)_3$, 4,8), 29.9 ($\text{C}(\text{CH}_3)_3$, $^{2,7/3,6}$), 29.8 ($\text{C}(\text{CH}_3)_3$, $^{3,6/2,7}$), 29.6 ($\text{C}(\text{CH}_3)_3$, 4,8) ppm. The carbonyl signal could not be detected.

$^{31}\text{P}\{^1\text{H}\}$ NMR (162 MHz, THF- d^8): $[\text{A}[\text{M}]_2\text{R}]_2\text{X}$ spin system (C_s , $R = 0.55\%$, for full parameter set s. Table 2): δ 89.41 (m, P^9 , 1P), -32.60 (m, $P^{2,7}$, 2P), -35.02 (m, $P^{3,6}$, 2P), -42.87 (m, $P^{4,8}$, 2P), -79.77 (m, $P^{1,5}$, 2P) ppm.

IR: $\tilde{\nu}$ 2952 (m), 2932 (m), 2889 (m), 2853 (m), 2022 (s, $\nu(\text{CO})$), 1964 (s, $\nu(\text{CO})$), 1743 (s, $\nu(\text{NO})$), 1456 (m), 1387 (w), 1357 (m), 1245 (w), 1168 (m), 1007 (w), 934 (w), 804 (m), 608 (w), 569 (m), 489 (m), 445 (m) cm^{-1} .

HR-ESI(+)-MS (THF): m/z 765.2252 $[\text{M} - \text{CO} - \text{NO}]^+$.

CHN, found: C, 43.64; H, 7.84; N, 1.27. $\text{C}_{30}\text{H}_{63}\text{CoNO}_3\text{P}_9$ requires C, 43.75; H, 7.71; N, 1.70%.

Synthesis of $[(\text{CuBr})_2\{\text{cyclo}-(\text{P}^4\text{Bu}_3)_2\text{P}^t\text{Bu}-\kappa^2\text{P}^2, \text{P}^7, \kappa^2\text{P}^3, \text{P}^6\}]$ (3)

A suspension of 85.47 mg (0.126 mmol) **L** and 71.84 mg (0.350 mmol, 2.77 equiv.) $[\text{CuBr}(\text{SMe}_2)]$ in 5 ml THF was heated to reflux for 0.5 min and then cooled to room temperature. The solvent was removed *in vacuo* and the residue was recrystallised in THF; at -60 °C yellow crystals formed. The mother liquor was decanted; after drying the crystals, 103.24 mg (0.100 mmol, 79%) **3**·THF were obtained.

Mp. loss of THF above 91 °C, decomposition above 238 °C.

^1H NMR (400 MHz, benzene- d^6): δ 3.57 (m, THF, 1.5H), 1.59 (d, C_4H_9 , 4,8 , $^3J_{\text{HP}} = 14.8$ Hz, 18H), 1.43 (m, C_4H_9 , 2,3,6,7 /THF 37.5H), 1.18 (d, C_4H_9 , 9 , $^3J_{\text{HP}} = 13.4$ Hz, 9H) ppm.

$^{13}\text{C}\{^1\text{H}\}$ NMR (101 MHz, benzene- d^6): δ 67.8 (s, THF), 35.7 (m, $\text{C}(\text{CH}_3)_3$, 2,3,6,7,9), 34.6 (m, $\text{C}(\text{CH}_3)_3$, 4,8), 32.5 (m, $\text{C}(\text{CH}_3)_3$, 4,8), 31.9 (m, $\text{C}(\text{CH}_3)_3$, 9), 29.2 (m, $\text{C}(\text{CH}_3)_3$, 2,3,6,7), 25.8 (s, THF) ppm.

$^{13}\text{C}\{^1\text{H}, ^{31}\text{P}\}$ NMR (101 MHz, benzene- d^6 , 28 °C): δ 67.8 (THF), 35.8 ($\text{C}(\text{CH}_3)_3$, 9), 35.7 ($\text{C}(\text{CH}_3)_3$, 2,3,6,7), 34.6 ($\text{C}(\text{CH}_3)_3$, 4,8), 32.5 ($\text{C}(\text{CH}_3)_3$, 4,8), 31.9 ($\text{C}(\text{CH}_3)_3$, 9), 29.2 ($\text{C}(\text{CH}_3)_3$, 2,3,6,7), 25.8 (THF) ppm.

$^{31}\text{P}\{^1\text{H}\}$ NMR (162 MHz, benzene- d^6): $[\text{A}[\text{M}]_2\text{R}]_2\text{X}$ spin system (C_{2v} , $R = 0.41\%$, for full parameter set s. Table 3): δ 34.27 (m, P^9 , 1P), 8.94 (m, $P^{4,8}$, 2P), -37.17 (m, $P^{2,3,6,7}$, 4P), -141.66 (m, $P^{1,5}$, 2P) ppm.

IR: $\tilde{\nu}$ 2942 (m), 2889 (m), 2855 (m), 1453 (s), 1392 (m), 1361 (s), 1211 (w), 1171 (s), 1065 (m), 1015 (w), 941 (w), 908 (w), 804 (m), 575 (w), 517 (m) cm^{-1} .

HR-ESI(+)-MS (THF): m/z 885.0303 $[\text{M} - \text{Br}]^+$, 1850.9805 $[\text{M}_2 - \text{Br}]^+$.

CHN, found: C, 37.53; H, 6.50; N, 0.00. $\text{C}_{28}\text{H}_{63}\text{Br}_2\text{Cu}_2\text{P}_9\cdot\text{C}_4\text{H}_8\text{O}$ requires C, 37.04; H, 6.90; N, 0.00%.

Synthesis of $[\text{RhCl}(\text{CO})\{\text{cyclo}-(\text{P}^4\text{Bu}_3)_2\text{P}^t\text{Bu}-\kappa^2\text{P}^6, \text{P}^9\}]$ (4)

70.37 mg (0.104 mmol) **L** and 20.15 mg (0.052 mmol, 0.50 equiv.) $[\{\text{RhCl}(\text{CO})_2\}_2]$ were stirred in 5 ml THF. Immediately, gas formation was observed. After 20 min, the solution was filtered and the solvent of the clear bright orange solution was removed *in vacuo*. The residue was washed with 2 ml *n*-pentane and dried at 60 °C *in vacuo*, yielding **4** (76.0 mg 0.090 mmol, 86%). Clear orange-red crystals suitable for single crystal X-ray diffraction were obtained by recrystallisation in THF.

Mp. decomposition above 183 °C.

^1H NMR (400 MHz, benzene- d^6): δ 1.69 (d, C_4H_9 , $^3J_{\text{HP}} = 14.9$ Hz, 9H), 1.60 (d, C_4H_9 , $^3J_{\text{HP}} = 18.1$ Hz, 9H), 1.53 (d, C_4H_9 , $^3J_{\text{HP}} = 13.3$ Hz, 9H), 1.50 (d, C_4H_9 , $^3J_{\text{HP}} = 17.3$ Hz, 9H), 1.32 (d, C_4H_9 , $^3J_{\text{HP}} = 13.2$ Hz, 9H), 1.14 (d, C_4H_9 , $^3J_{\text{HP}} = 13.4$ Hz, 9H), 1.08 (d, C_4H_9 , $^3J_{\text{HP}} = 13.7$ Hz, 9H) ppm. Assignment of the signals is not possible due to their equal intensities and their appearance in the same region of the spectrum.

$^{13}\text{C}\{^1\text{H}\}$ NMR (101 MHz, benzene- d^6): δ 41.8 (m, $\text{C}(\text{CH}_3)_3$, 9), 35.1 (m, $\text{C}(\text{CH}_3)_3$), 29.9 (d, $\text{C}(\text{CH}_3)_3$, $^3J_{\text{CP}} = 15.1$ Hz), 29.4 (m, $\text{C}(\text{CH}_3)_3$), 29.2 (d, $\text{C}(\text{CH}_3)_3$, $^3J_{\text{CP}} = 14.3$ Hz), 28.6 (d, $\text{C}(\text{CH}_3)_3$, $^3J_{\text{CP}} = 10.4$ Hz), 27.5 (m, $\text{C}(\text{CH}_3)_3$) ppm. Full assignment of the signals is not possible. Due to their equal intensities and their appearance in the same region of the spectrum, it is only distinguished between quaternary and primary carbons. The same applies to the $^{13}\text{C}\{^1\text{H}, ^{31}\text{P}\}$ NMR spectrum.

$^{13}\text{C}\{^1\text{H}, ^{31}\text{P}\}$ NMR (101 MHz, benzene- d^6 , 28 °C): δ 41.7 ($\text{C}(\text{CH}_3)_3$, 9), 35.1 ($\text{C}(\text{CH}_3)_3$), 33.5 ($\text{C}(\text{CH}_3)_3$), 32.4 ($\text{C}(\text{CH}_3)_3$), 32.0 ($\text{C}(\text{CH}_3)_3$), 31.4 ($\text{C}(\text{CH}_3)_3$), 29.8 ($\text{C}(\text{CH}_3)_3$), 29.4 ($\text{C}(\text{CH}_3)_3$), 29.2 ($\text{C}(\text{CH}_3)_3$), 29.0 ($\text{C}(\text{CH}_3)_3$), 28.5 ($\text{C}(\text{CH}_3)_3$), 27.5 ($\text{C}(\text{CH}_3)_3$), 27.4 ($\text{C}(\text{CH}_3)_3$) ppm. One $\text{C}(\text{CH}_3)_3$ signal could not be detected.

$^{31}\text{P}\{^1\text{H}\}$ NMR (162 MHz, benzene- d^6): δ 17.5 (m, P^6 , 1P), 5.0 (m, P^4 , 1P), -6.6 (m, P^9 , 1P), -27.9 (m, P^3 , 1P), -30.7 (m, P^7 , 1P), -41.5 (m, P^2 , 1P), -50.3 (m, P^8 , 1P), -94.4 (m, P^5 , 1P), -96.7 (m, P^1 , 1P) ppm.

IR: $\tilde{\nu}$ 2955 (m), 2934 (m), 2888 (m), 2854 (m), 2038 (w), 1997 (s, $\nu(\text{CO})$), 1951 (w), 1932 (w), 1470 (m), 1455 (s), 1387 (m), 1357 (s), 1169 (s), 1068 (w), 1008 (m), 934 (w), 803 (m), 618 (w), 593 (w), 570 (w), 528 (m), 520 (m), 492 (m), 453 (m), 432 (m) cm^{-1} .

HR-ESI(+)-MS (THF): m/z 797.1558 $[\text{M} - \text{CO} - \text{Cl} + \text{O}]^+$.

CHN, found: C, 41.47; H, 7.63; N, 0.00. $\text{C}_{29}\text{H}_{63}\text{ClOP}_9\text{Rh}$ requires C, 41.22; H, 7.52; N, 0.00%.

Synthesis of $[\text{PdCl}_2\{\text{cyclo}(\text{P}_4^t\text{Bu}_3)_2\text{P}^t\text{Bu}-\kappa^2\text{P}^6, \text{P}^9\}]$ (5)

A solution of 15.68 mg (0.021 mmol) $\{\text{cyclo}(\text{P}_4^t\text{Bu}_3)_2\text{P}^t\text{Bu}$ in 3 ml THF was added to 12.22 mg (0.043 mmol, 2.01 equiv.) $[\text{PdCl}_2(\text{COD})]$ (COD = cycloocta-1,5-diene). The solution was heated to 60 °C for 5 d. The solvent was removed *in vacuo* and the residue was extracted with 10 ml THF. After removal of the solvent, the remaining red-orange solid was dissolved in 5 ml toluene/THF (3:2 (v/v)). The resulting solution was filtered and stored at 4 °C yielding pale yellow single crystals of 5 suitable for X-ray structure determination.

Further characterisation was not possible due to decomposition of the compound in solution.

Crystallography

Single crystal X-ray diffraction data were collected with a GEMINI CCD diffractometer (RIGAKU). The radiation source was a molybdenum anode (Mo- K_{α} , $\lambda = 0.71073$ Å). The data reduction was carried out with CrysAlis Pro⁷¹ using an empirical absorption correction with spherical harmonics (SCALE3 ABSPACK). All structures were solved by dual space methods with SHELXT.⁷² Structure refinement was done with SHELXL⁷³ by using full-matrix least-square routines against F^2 and anisotropic refinement of all non-hydrogen atoms. All hydrogen atoms were calculated on idealised positions. The pictures were generated with the programme Mercury.⁷⁴ In all pictures, hydrogen atoms were omitted for clarity and thermal ellipsoids are shown with 50% probability. Crystallographic data and the CCDC code for the single crystal structures reported here are listed in Table S2 (ESI†).

Conflicts of interest

There are no conflicts to declare.

Acknowledgements

Financial support from the Studienstiftung des deutschen Volkes (doctoral grant for VJE) is gratefully acknowledged.

References

- 1 K. B. Dillon, F. Mathey and J. F. Nixon, *Phosphorus: The Carbon Copy. From Organophosphorus to Phospha-organic Chemistry*, Wiley, Chichester, 1998.
- 2 M. Baudler, *Angew. Chem., Int. Ed. Engl.*, 1982, **21**, 492.
- 3 M. Baudler and K. Glinka, *Chem. Rev.*, 1993, **93**, 1623.
- 4 V. J. Eilrich and E. Hey-Hawkins, *Coord. Chem. Rev.*, 2021, **437**, 213749 and the references therein.
- 5 T. Wellnitz and C. Hering-Junghans, *Eur. J. Inorg. Chem.*, 2021, 8.
- 6 G. Fritz, H.-W. Schneider, W. Hönle and H. G. von Schnering, *Z. Anorg. Allg. Chem.*, 1990, **585**, 51.
- 7 G. Fritz, B. Mayer and E. Matern, *Z. Anorg. Allg. Chem.*, 1992, **608**, 7.
- 8 G. Fritz and B. Mayer, *Z. Anorg. Allg. Chem.*, 1992, **610**, 51.
- 9 J. Queisser, D. Fenske, B. Lehari and H. Oesen, *Z. Anorg. Allg. Chem.*, 1994, **620**, 1821.
- 10 J. Queisser and D. Fenske, *Z. Anorg. Allg. Chem.*, 1994, **620**, 58.
- 11 E. Charalambous, L. Heuer, B. F. Johnson, J. Lewis, W.-S. Li, M. McPartlin and A. D. Massey, *J. Organomet. Chem.*, 1994, **468**, C9–C12.
- 12 H. Wunderlich, *Z. Kristallogr.*, 1995, **210**, 889.
- 13 H. Wunderlich, *Z. Kristallogr.*, 1995, **210**, 632.
- 14 H.-G. Ang, L.-L. Koh and Q. Zhang, *J. Chem. Soc., Dalton Trans.*, 1995, 2757.
- 15 H.-G. Ang, S.-G. Ang, W.-L. Kwik and Q. Zhang, *J. Organomet. Chem.*, 1995, **485**, C10–C13.
- 16 D. Fenske, J. Queisser and H. Schottmüller, *Z. Anorg. Allg. Chem.*, 1996, **622**, 1731.
- 17 H.-G. Ang, S.-G. Ang and Q. Zhang, *Phosphorus, Sulfur Silicon Relat. Elem.*, 1996, **109**, 145.
- 18 D. Fenske and H. Schottmüller, *Z. Anorg. Allg. Chem.*, 1998, **624**, 443.
- 19 A. Deeg and H. Wunderlich, *Acta Crystallogr., Sect. C: Cryst. Struct. Commun.*, 1998, **54**, IUC9800054.
- 20 H. Krautscheid, E. Matern, J. Olkowska-Oetzel, J. Pikies and G. Fritz, *Z. Anorg. Allg. Chem.*, 2001, **627**, 2118.
- 21 H.-G. Ang, K.-W. Ang, S.-G. Ang and A. L. Rheingold, *J. Chem. Soc., Dalton Trans.*, 1996, 3131.
- 22 H.-G. Ang, S.-G. Ang and Q. Zhang, *J. Chem. Soc., Dalton Trans.*, 1996, 2773.
- 23 H.-G. Ang, S.-G. Ang and Q. Zhang, *J. Chem. Soc., Dalton Trans.*, 1996, 3843.
- 24 R. M. de Silva, M. J. Mays, P. R. Raithby and G. A. Solan, *J. Organomet. Chem.*, 2002, **642**, 237.
- 25 D. M. Yufanyi, T. Grell, M.-B. Sárosi, P. Lönnecke and E. Hey-Hawkins, *Pure Appl. Chem.*, 2019, **91**, 785.
- 26 D. M. Yufanyi, T. Grell and E. Hey-Hawkins, *Eur. J. Inorg. Chem.*, 2019, 1557.
- 27 R. Schmidt, S. A. Moya, D. Villagra, H. Binder and G. Heckmann, *Bol. Soc. Chil. Quim.*, 1996, **41**, 371.
- 28 R. Ahlrichs, D. Fenske, H. Oesen and U. Schneider, *Angew. Chem., Int. Ed. Engl.*, 1992, **31**, 323.
- 29 T. Grell and E. Hey-Hawkins, *Inorg. Chem.*, 2020, **59**, 7487.
- 30 T. Grell and E. Hey-Hawkins, *Chem. – Eur. J.*, 2020, **26**, 1008.
- 31 S. J. Geier and D. W. Stephan, *Chem. Commun.*, 2008, 2779.
- 32 R. G. Pearson, *J. Am. Chem. Soc.*, 1963, **85**, 3533.
- 33 M. Baudler, Y. Aktalay, K.-F. Tebbe and T. Heinlein, *Angew. Chem., Int. Ed. Engl.*, 1981, **20**, 967.

- 34 T. Grell and E. Hey-Hawkins, *Eur. J. Inorg. Chem.*, 2020, 732.
- 35 M. Baudler, M. Schnalke and C. Wiaterek, *Z. Anorg. Allg. Chem.*, 1990, **585**, 7.
- 36 V. J. Eilrich, T. Grell, P. Lönnecke and E. Hey-Hawkins, *Dalton Trans.*, 2021, **50**, 14144.
- 37 D. Dou, E. N. Duesler and R. T. Paine, *Inorg. Chem.*, 1999, **38**, 788.
- 38 W. S. Sheldrick, S. Morton and O. Stelzer, *Z. Anorg. Allg. Chem.*, 1981, **475**, 232.
- 39 Y. W. Li, M. G. Newton, N. K. Bhattacharyya and R. B. King, *Inorg. Chem.*, 1992, **31**, 2069.
- 40 G. Fritz and K. Stoll, *Rev. Roum. Chim.*, 1986, **31**, 949.
- 41 M. Baudler and H. Tschäbunin, *Z. Anorg. Allg. Chem.*, 1984, **511**, 77.
- 42 J. P. Albrand, A. Cogne and J. B. Robert, *J. Am. Chem. Soc.*, 1978, **100**, 2600.
- 43 H. J. Bernstein, J. A. Pople and W. G. Schneider, *Can. J. Chem.*, 1957, **35**, 67.
- 44 R. E. Richards and T. Schaefer, *Mol. Phys.*, 1958, **1**, 331.
- 45 C. W. Haigh, *J. Chem. Soc. A*, 1970, 1682.
- 46 S. Berger, S. Braun and H.-O. Kalinowski, *NMR-Spektroskopie von Nichtmetallen Bd. 3. ³¹P-NMR-Spektroskopie*, Thieme, Stuttgart, 1993.
- 47 J. Ellermann, N. Will and F. Knoch, *J. Organomet. Chem.*, 1989, **366**, 197.
- 48 J. Ellermann, E. Köck, H. Zimmermann and M. Gomm, *J. Organomet. Chem.*, 1988, **345**, 167.
- 49 V. G. Albano, P. L. Bellon and G. Ciani, *J. Organomet. Chem.*, 1972, **38**, 155.
- 50 F. S. Mortimer, *J. Magn. Reson. (1969–1992)*, 1969, **1**, 1.
- 51 V. J. Eilrich, T. Grell, P. Lönnecke, C. Song, J. Matysik and E. Hey-Hawkins, *Dalton Trans.*, 2022, **51**, 4627.
- 52 B. Riegel, A. Pfitzner, G. Heckmann, H. Binder and E. Fluck, *Z. Anorg. Allg. Chem.*, 1995, **621**, 1365.
- 53 A. Kircali, R. Frank, S. Gómez-Ruiz, B. Kirchner and E. Hey-Hawkins, *ChemPlusChem*, 2012, **77**, 341.
- 54 A. Kircali Akdag, P. Lönnecke and E. Hey-Hawkins, *Z. Anorg. Allg. Chem.*, 2014, **640**, 271.
- 55 H. O. House, C.-Y. Chu, J. M. Wilkins and M. J. Umen, *J. Org. Chem.*, 1975, **40**, 1460.
- 56 E. Speyer and H. Wolf, *Ber. Dtsch. Chem. Ges. B*, 1927, **60**, 1424.
- 57 W. P. Fehlhammer, W. A. Herrmann and K. Öfele, in *Handbuch der Präparativen Anorganischen Chemie. In drei Bänden. Dritter Band*, ed. G. Brauer, Ferdinand Enke Verlag, Stuttgart, 3rd edn, 1981, vol. 3, pp. 1799–2033.
- 58 J. A. McCleverty and G. Wilkinson, in *Inorganic Syntheses: Reagents for Transition Metal Complex and Organometallic Syntheses*, ed. F. Basolo and R. J. Angelici, Wiley, New York, 1990, vol. 28, pp. 84–86.
- 59 D. Drew, J. R. Doyle and A. G. Shaver, in *Inorganic Syntheses: Reagents for Transition Metal Complex and Organometallic Syntheses*, ed. F. Basolo and R. J. Angelici, Wiley, New York, 1990, vol. 28, pp. 346–349.
- 60 R. K. Harris, E. D. Becker, S. M. Cabral De Menezes, R. J. Goodfellow and P. Granger, *Concepts Magn. Reson.*, 2002, **14**, 326.
- 61 C. Ammann, P. Meier and A. E. Merbach, *J. Magn. Reson. (1969–1992)*, 1982, **46**, 319.
- 62 *DAISY, part of TopSpin 4.1.1*, Bruker BioSpin GmbH, Rheinstetten, 2020.
- 63 F. Neese, *Wiley Interdiscip. Rev.: Comput. Mol. Sci.*, 2018, **8**, e1327.
- 64 E. Caldeweyher, C. Bannwarth and S. Grimme, *J. Chem. Phys.*, 2017, **147**, 34112.
- 65 E. Caldeweyher, S. Ehlert, A. Hansen, H. Neugebauer, S. Spicher, C. Bannwarth and S. Grimme, *J. Chem. Phys.*, 2019, **150**, 154122.
- 66 C. van Wüllen, *J. Chem. Phys.*, 1998, **109**, 392.
- 67 J. Tao, J. P. Perdew, V. N. Staroverov and G. E. Scuseria, *Phys. Rev. Lett.*, 2003, **91**, 146401.
- 68 V. N. Staroverov, G. E. Scuseria, J. Tao and J. P. Perdew, *J. Chem. Phys.*, 2003, **119**, 12129.
- 69 D. A. Pantazis, X.-Y. Chen, C. R. Landis and F. Neese, *J. Chem. Theory Comput.*, 2008, **4**, 908.
- 70 V. Barone and M. Cossi, *J. Phys. Chem. A*, 1998, **102**, 1995.
- 71 *Agilent, CrysAlis PRO*, Agilent Technologies Ltd., Yarnton, 2019.
- 72 G. M. Sheldrick, *Acta Crystallogr., Sect. A: Found. Adv.*, 2015, **71**, 3.
- 73 G. M. Sheldrick, *Acta Crystallogr., Sect. C: Struct. Chem.*, 2015, **71**, 3.
- 74 C. F. Macrae, I. J. Bruno, J. A. Chisholm, P. R. Edgington, P. McCabe, E. Pidcock, L. Rodriguez-Monge, R. Taylor, J. van de Streek and P. A. Wood, *J. Appl. Crystallogr.*, 2008, **41**, 466.